Spatial Light Modulators for Complex Spatiotemporal Illumination of Neuronal Networks

Chapter *in* Neuromethods · December 2011

DOI: 10.1007/7657_2011_3

6 authors, including:

Francesco Difato
Istituto Italiano di Tecnologia
66 PUBLICATIONS **1,050** CITATIONS
SEE PROFILE

Marco Dal Maschio
University of Padova
73 PUBLICATIONS **2,213** CITATIONS
SEE PROFILE

Riccardo Beltramo
UCSF University of California, San Francisco
30 PUBLICATIONS **668** CITATIONS
SEE PROFILE

Axel Blau
Startup Innovativa
63 PUBLICATIONS **1,652** CITATIONS
SEE PROFILE

Neuromethods (2011)
DOI 10.1007/7657_2011_3

1

Spatial Light Modulators for Complex Spatiotemporal Illumination of Neuronal Networks

2
3

Francesco Difato, Marco Dal Maschio, Riccardo Beltramo, Axel Blau, Fabio Benfenati, and Tommaso Fellin

4
5

Abstract

6

The introduction of fluorescent probes and light-sensitive molecules and the recent development of optogenetics are tremendously contributing to our understanding of neuronal circuit function. In parallel with the development of these optical tools, new technologies for the illumination of neural tissue with complex spatiotemporal patterns have been introduced. Here, we describe a method for generating spatially modulated illumination by using liquid crystal on silicon spatial light modulators (LCOS-SLMs). The theoretical background and the description of working principles of LCOS-SLMs are presented together with a detailed experimental procedure to install LCOS-SLMs on conventional two-photon laser scanning microscopes and perform experiments on neuronal cells. In combination with the development of light-sensitive proteins with cell-specific and subcellularly localized expression, this technical approach has the potential to open new horizons for the optical investigation of neuronal circuits.

7
8
9
10
11
12
13
14
15
16
17

Key words: Digital holography, Structured light, Two-photon microscopy, Imaging, Photostimulation, Uncaging

18
19

1. Introduction

20

Due to its low invasiveness and the ability to monitor large numbers of cells while maintaining single-cell resolution, optical microscopy currently represents a fundamental tool for the investigation of the central nervous system. In particular, the combination of optical microscopy with the development of fluorescent indicators, caged compounds, and genetically engineered light-sensitive proteins (1–7) is bringing new and previously unachievable insights into neuronal network function in vitro as well as in the intact brain. Currently, the two most common configurations of optical microscopy used in neuroscience laboratories are wide-field illumination and laser scanning imaging. In wide-field microscopy, the whole

21
22
23
24
25
26
27
28
29
30
31

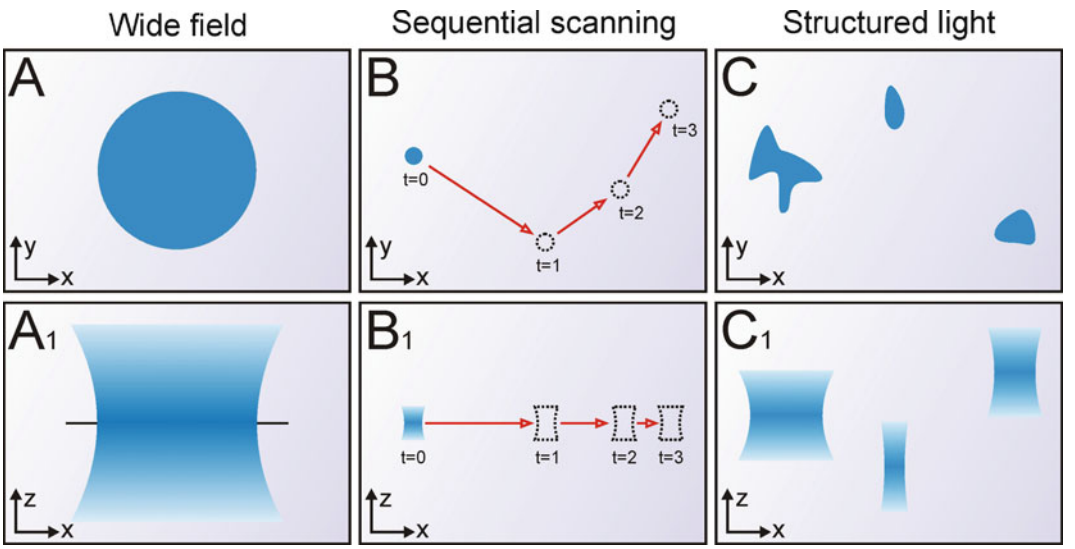

Fig. 1. Advantages of structured light illumination. (**a**, **b**) While wide-field microscopy (a) results in the illumination of the whole field of view (*blue disk*) preventing the projection of complex spatial patterns, in scanning imaging (b) the image is formed by sequentially illuminating the field of view with a diffraction-limited spot (*blue disk*, $t = 0$) which is steered across the sample (*open circles*, $t = 1, 2, 3$) according to the desired trajectory (*red arrows*). (**c**) Structured light illumination offers the possibility to shape the light in the *x*–*y* plane to any desired pattern, thus simultaneously illuminating complex structures at the sample plane. (**a_1–c_1**) The *x*–*z* profiles under the different experimental conditions are shown. Note that with structured light complex three-dimensional patterns can be obtained and the compression of the *z* dimension of different *x*–*y* shapes can be achieved with temporal focusing (41, 49) (see also Sect. 6).

field of view is simultaneously illuminated, allowing fast image acquisition or fast repetitive stimulation, but preventing the application of complex spatial light patterns (Fig. 1a). Differently, in laser scanning microscopy, a diffraction-limited laser spot is sequentially deflected in the field of view, allowing the selective illumination of portions of the sample that depend on the scanning trajectory (Fig. 1b). This configuration leads to an increase of the spatial but to a significant loss in the time resolution of the optical system. Both approaches, thus, have intrinsic limitations with respect to the degree of complexity with which spatiotemporal patterns of light can be projected onto the biological sample. Illumination with structured light represents an innovative alternative to overcome these limitations. In this experimental approach, the laser wave front is engineered (or shaped) to simultaneously and selectively illuminate only specific regions of interest in a given field of view (Fig. 1c). This technique offers flexibility in the pattern of illumination that cannot be achieved with more traditional optical approaches and gives the opportunity of imaging/stimulating simultaneously multiple portions of a given cell or different cells within a neuronal network.

Over the course of years, various techniques have been developed to sculpt the light wave front (8–10), including phase modulation

of the laser beam. Initially applied in astronomy to develop adaptive systems to correct optical aberration induced by atmospheric turbulence (11, 12) or to filter out the effects of specimen-induced aberrations (13), light phase modulation has been more recently applied to the investigation of the nervous system (14). Among different devices that generate phase modulation (15), liquid crystals on silicon spatial light modulators (LCOS-SLMs) are increasingly recognized as preferred tools. These devices have been largely used for optical tweezers applications (16–21) and more recently rediscovered as active tools for distortion minimization in two-photon in vivo microscopy (22, 23) or to perform imaging or photostimulation of neuronal circuits with complex spatiotemporal patterns (14, 24, 25). In this chapter, we present the theory of operation of LCOS-SLMs together with a detailed experimental protocol for their integration into commercially available scanning microscopes for functional imaging/uncaging experiments on neuronal networks with sculpted light.

1.1. Light Wave Front as the Superposition of Multiple Spherical Components

The working principle of wave-front engineering with LCOS-SLMs is based on the Huygens principle, which states that an arbitrary wave front can be considered as the envelope of spherical waves emitted by point sources. In this view, the calculation of the complex field distribution $U(x,y)$ at a certain distance z in the propagation direction is obtained from the integration of a set of spherical waves generated by a collection of points in the source plane $\Sigma(\xi,\zeta)$ at $z = 0$ as given by the Huygens–Fresnel diffraction formula (26):

$$U(x,y) = \frac{1}{j\lambda} \iint_{\Sigma} U(\xi,\zeta) \frac{e^{jkr}}{r} \cos\beta \, \mathrm{d}s,$$

where $U(\xi,\zeta)e^{jkr}/r$ is the diverging spherical wave originating in the point (ξ,ζ), separated by a distance r from the point (x,y) in the observation plane, β the angle formed by the vector r and the z direction, j the imaginary unit, k the wave number, and λ the light wavelength (Fig. 2). The previous diffraction formula, rearranged by considering $\cos\beta$ as the z/r ratio and taking into account the expression for r derived by its Taylor series truncated at the quadratic term, in the far-field approximation, results in the following Fraunhofer diffraction integral:

$$U(x,y) = \frac{e^{jkz}}{j\lambda z} e^{j\frac{k}{2z}(x^2+y^2)} \iint_{-\infty}^{+\infty} U(\xi,\zeta) e^{-j\frac{2\pi}{\lambda z}(x\xi+y\zeta)} \mathrm{d}\xi \, \mathrm{d}\zeta.$$

Besides the first quadratic phase factor, the last equation describes $U(x,y)$ as the two-dimensional Fourier transform of the initial complex field distribution $U(\xi,\zeta)$ and demonstrates that the amplitude and phase of the complex field at coordinates (x, y)

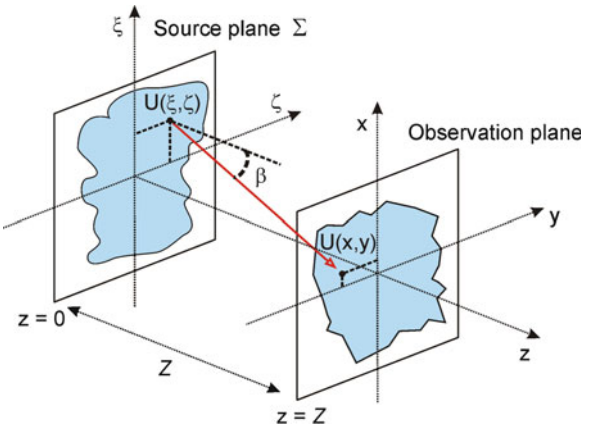

Fig. 2. Light propagation between Fourier planes. The complex field distribution $U(x,y)$ at a certain distance Z in the direction of propagation results from the integration of spherical waves generated by a collection of points in the source plane at $z = 0$.

in the observation plane are determined by the input Fourier components at frequencies $(x/\lambda z, y/\lambda z)$ in the source plane (26). As a consequence, a certain diffraction pattern observed in the far field is determined by the propagation of a specific wave front generated by a proper map of spatial frequency components. Considering a condition of uniform illumination, this map of spatial frequencies is completely described by a distribution of phase delays within the illuminated area at the source plane.

1.2. Shaping the Light Wave Front by Phase Modulation with LCOS-SLMs

In light of the theory described in the previous section, it is clear that an effective strategy to engineer a light wave front is by modulating the phase of its spherical components (Fig. 3a). To achieve this aim, current technology has focused on certain kinds of birefringent materials in which a change in molecular orientation results in a change in the effective refraction index. This is the case for nematic liquid crystals which are commonly used as components of LCOS-SLMs devices (Fig. 3b). Indeed, nematic liquid crystals have typically a rod-like molecular structure with one unique symmetry axis of anisotropy, called optic axis or director. This leads to the existence of two different refractive indices for different polarizations, an extraordinary refractive index (n_e) for light polarized perpendicularly to the optic axis, and an ordinary refractive index (n_o) for light polarized in parallel to the optic axis (Fig. 3c). LCOS-SLMs are composed of a matrix of active cells, each containing nematic liquid crystals the orientation of which can be individually controlled through the application of a voltage difference (Fig. 3b). Considering a cell where the liquid crystal molecules are all aligned with one another, when an electric field is applied across the liquid crystal layer along the light

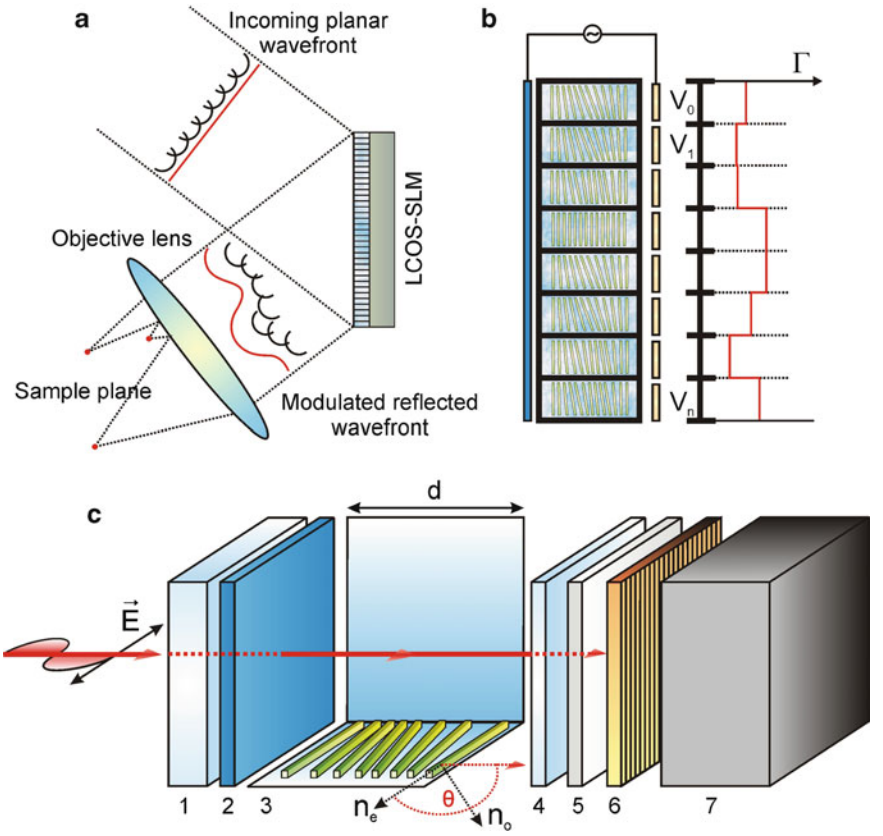

Fig. 3. LCOS-SLM working principle. (**a**) Schematic view of the effect of an LCOS-SLM in shaping an incident planar laser wave front (*red straight line*). By modulating the phase of the spherical components (*black semicircles*), the LCOS-SLM modifies the wave front of the reflected light beam (*curved red line*). This change in phase that is introduced in the Fourier space by the LCOS-SLM results in the generation of structured light illumination at the sample plane (behind the objective lens). (**b**) Zoom in showing the structure of the LCOS-SLM as a matrix of active cells. By controlling the liquid crystal orientation through voltage, each cell (or pixel) can differentially modulate the phase of the light (Γ) impinging upon it. (**c**) The structure of a single cell is shown at an expanded scale. *Legend*: (1) protective cover glass, (2) transparent indium thin oxide (ITO) electrode layer, (3) liquid crystal layer, (4) backplane alignment layer, (5) planar dielectric mirror, (6) electrode pixel matrix of aluminum pads, (7) complementary metal oxide semiconductor (CMOS) driving circuitry.

propagation direction (z), a progressive point-by-point reorientation of the molecules occurs and a change in the effective refraction index n_{eff} profile is induced according to the following equation:

$$n_{eff}(\theta(z)) = \frac{n_o n_e}{\sqrt{n_o^2 \sin^2\vartheta(z) + n_e^2 \cos^2\vartheta(z)}},$$

where ϑ is the angle between the director and the direction of light propagation. Because the degree of reorientation depends on the z position within the liquid crystal layer, the total phase delay Γ generated by a cell of thickness d results from the following integration (27, 28):

$$\Gamma = \frac{2\pi}{\lambda} \int_{-d/2}^{+d/2} (n_{eff}(\vartheta(z)) - n_o)\mathrm{d}z.$$

It is, thus, clear that the response of the director distribution, $\vartheta(z)$, to the application of external fields and the time required for liquid crystal reorientation represent the most important features determining the performance of a liquid crystal cell, both in terms of the reliability and precision of the phase modulation and in terms of the refresh rate.

An analytical expression for the time and voltage dependencies of the phase delay $\Gamma(t, V)$ is based on approximated solutions of the Oseen–Frank (29) and Ericksen–Leslie set of equations (30). It is derived by minimizing the total free energy of the system, including the elastic and viscous components. For a specific liquid crystal compound, the solution of these equations shows that (1) a bias potential greater than the Frèedericksz threshold has to be applied across the liquid crystal cell in order to induce molecule reorientation (30). (2) The cell modulation capability in terms of π fractions, also called phase stroke, depends on the ratio between the cell thickness d and the wavelength λ, and is proportional to the material birefringence $n_e - n_o$. (3) Nematic liquid crystal molecules have typical settling times that are proportional to the square of the cell thickness d and to the viscosity coefficient η while they are inversely proportional to the splay elastic constant (29). All these parameters must be considered in the design of liquid crystal-based SLMs and contribute to define the temporal and optical performance (i.e., the maximum refresh rate and the spectral range) of the device.

1.3. Structure of Commercial LCOS-SLMs

The core of reflective LCOS-SLMs (Fig. 3c) is a matrix of active pixels, each generally composed of (1) a protective cover glass with an antireflection broadband or specific coating; (2) a transparent indium thin oxide (ITO) layer serving as ground electrode and being rubbed or coated by a vapor-deposited SiO2 alignment layer to provide the proper director orientation and pretilting angle for liquid crystal molecules; (3) the liquid crystal layer; (4) a backplane alignment layer; (5) a planar dielectric mirror which enhances the light utilization efficiency and the fill factor; (6) a layer with aluminum electrode pads forming the pixel matrix; and (7) the complementary metal oxide semiconductor (CMOS) driving and addressing circuitry realized with very large-scale integration (VLSI) technology. Depending on the reciprocal orientation of the two alignment layers, the direction of the external electric field, and the polarization state of the incoming light, LCOS-SLMs operate in different modulation modes. In particular, for the configuration with parallel alignment layers, pure phase ($\alpha = 0°$), or a

combination of phase and amplitude ($0 < \alpha < 90°$), modulation can be achieved by altering the angle α between the polarization of the incoming light and the liquid crystal optical axis (see Sect. 1). Commercial two-dimensional liquid crystal matrices with layouts ranging from 256 × 256 to 1900 × 1,000 and pixel sizes ranging between 8 × 8 and 40 × 40 μm^2 have an effective active area of the order of several mm^2 and maximum spatial resolutions in the range of 20–33 line pairs/mm (9). LCOS-SLMs are currently available with optical windows covering wavelengths ranging from UV to IR and are subjected to a calibration process to linearly map the 8-bit levels to the designed phase stroke for each specific wavelength.

1.4. Structured Light Illumination for the Optical Investigation of Neuronal Function

Initially applied to aberration correction optics and for designing optical tweezers (see Sect. 1), LCOS-SLM technology has been recently applied to the study of the central nervous system. Single-photon holographic uncaging of caged 4-methoxy-7-nitroindolinyl-caged-L-glutamate (MNI-glutamate) has been performed on cerebellar and hippocampal neurons in brain slice preparation in combination with intracellular recordings to measure photoactivation-induced currents mediated by the α-amino-3-hydroxyl-5-methyl-4-isoxazole-propionate (AMPA) receptor. These initial studies demonstrated that the shaping of the excitation light combined with classical electrophysiology recordings represents an extremely useful tool for the functional mapping of ion channels' distribution throughout different subcellular compartments (14). In a similar experimental approach, but using two- rather than single-photon excitation, localized photostimulation of dendritic spines with holographic illumination has demonstrated the potentials of this technique for studying neuronal input summation properties and suprathreshold activation of pyramidal neurons in brain slices (25). Besides electrophysiological recordings, holographic uncaging experiments have been performed in combination with Ca^{2+} imaging to detect and characterize the activation of AMPA receptors in glial cells in hippocampal slices. In this study, an image quality enhancement method was introduced to generate holographic illumination based on reliable volumetric rendering of the cell soma distribution, which was derived from wide-field excitation stacks (24). Two-photon holographic illumination has not only been used for photoactivation or photo-uncaging experiments, but also for fast scanless fluorescence imaging both in vitro and in situ (25, 31). This particular application of SLM-based microscopy allows the simultaneous imaging of multiple regions of interest (as for example different neurons or different portions of a neuron) in a given field of view at high acquisition frequency (tens to hundreds of Hz).

Recent technical advances in this field of research include a portable holographic microscope (32) and a dual microscope,

which combines two independently tunable lasers with an SLM-based holographic module and a conventional scan head. This latter system combines the versatility of scanless holographic excitation for imaging or photostimulation together with the reliability of standard galvo-steered spot uncaging and high-resolution multiphoton scanning imaging (31). The dual microscope can be used in two principal configurations: holographic imaging combined with galvo-steered uncaging and conventional scanning imaging combined with structured light uncaging. The potentials of this system for the study of brain function have been demonstrated with MNI-glutamate uncaging and Ca^{2+} imaging experiments on neuronal cultures (31).

1.5. Present and Future Perspectives

Structured light illumination obtained with LCOS-SLM technology offers many advantages when compared to common imaging and photostimulating approaches. Traditional point scanning systems based on galvo mirror devices or innovative beam steering configurations with acousto-optical deflectors are highly reliable and unparalleled in their switching rates. Nonetheless, they are limited by being single-spot illumination techniques which do not allow the simultaneous illumination of the sample at multiple locations or with arbitrary two/three-dimensional patterns (Fig. 1, see also Sect. 2). These considerations become particularly relevant in applications, where the low spatial density and the fast temporal relaxation dynamics of light-excited molecules are main factors determining the efficacy of the optical stimulation (33). For example, structured light illumination obtained with temporal focusing (to achieve thin, disk-like stimulation volumes with lateral diameters two orders of magnitude larger than diffraction-limited spots, see Sect. 6) has been used for efficient two-photon excitation of Channelrhodopsin 2 (34). From this point of view, the flexible beam shaping capabilities provided by holographic microscopy based on LCOS-SLMs represent a very promising technical approach to be used in combination with optogenetics and, more in general, with photoactivable proteins which may require complex patterns of stimulation. Indeed, a recent study (35) shows effective two-photon stimulation of channelrhodopsin with structured light illumination with modulation techniques derived from the theory of the phase contrast (36, 37) highlighting the importance of this approach for the activation of sparse neuronal assemblies with complex spatiotemporal patterns (33).

For imaging applications, holographic excitation systems can be used to illuminate arbitrary regions of interest within the field of view while simultaneously detecting the emitted fluorescence with a fast CCD camera. The major advantage of this parallel approach is its high acquisition rate, which is only limited by the signal-to-noise (S/N) ratio of the excited fluorescence and the camera frame rate. It, thus, outperforms acquisition system based on the

combination of galvo mirror scanning and photomultiplier tube detection. For example, if a field of view is divided into a 512 × 512 pixel array and scanned with a 4.4-μs dwell time per pixel, a frame rate lower than one frame per second (fps) is obtained. In contrast, using a scanless holographic configuration on both brain slices and cultured neuron preparations, spontaneous Ca^{2+} signals recorded with acquisition rates up to 70 fps have been reported (25, 31).

The considerations discussed above together with the prospects that future generation of LCOS-SLMs will have even higher refresh rates and larger spectral windows suggest that single- and multiphoton structured light illumination offers unique advantages compared to more traditional optical approaches. In combination with genetically encoded and cell-specific indicators/actuators, the complexity of the light stimuli and the flexibility with which they can be applied to the sample with this technique promise to bring new and fundamental insights into our understanding of brain circuits.

2. Materials

- Opto-mechanics for mounting freestanding optics and cage assembly, including bases (e.g., BA1, Thorlabs Inc., Newton, NJ), post holders (PH1/M–PH6/M), posts (TR20/M–TR300/M), right-angled clamps (RA90/M), flipping mounts (FM90), kinematic mounts (KM100/KCB1), cage assembly rods (ER8-ER05), square cage plates (CP02/M).
- High reflective ($R > 99\%$) NIR dielectric mirrors (BB1-E03) (Thorlabs Inc., Newton, NJ).
- Mounted achromatic IR lenses (AC254-100-B-ML, AC254-300-B-ML, AC254-100-B-ML, AC254-030-B-ML) (Thorlabs Inc., Newton, NJ).
- Half waveplate (lambda/2 B. Halle Nachfl GmbH).
- Research grade upright biological/life science optical microscope (Olympus BX61W, Milan, Italy) with the following components: bright-field illumination assembly in transmission (halogen bulb); fluorescence illumination assembly (mercury lamp); rotating filter wheel for filter cubes, Z objective motorization; objectives 20× XLUMPLFL20XW 0.95 NA, 40× LUMPLFL40XW 0.8 NA, 60× LUMFL, 1.1 NA.
- Two-photon system Ultima IV from Prairie Technologies (Madison, WI) with the following main components: Chameleon Ultra II Ti:Sapphire source (Coherent, Milan, Italy);

Pockels cell modulator (350–80 LA-BK, Conoptics, Danbury, CT); scanhead equipped with short pass dichroic mirror (FF670-SDi01, Semrock, Rochester, NJ), IR blocking filter (ET750sp-2p8), and emission filters 530/50 nm and 590/40 nm (Chroma, Fuerstenfeldbruck, Germany).

- Orca R2 CCD camera (Hamamatsu, Milan, Italy).
- Reflective X10468-07 LCOS spatial light modulator (Hamamatsu, Milan, Italy).
- CARPE Autocorrelator with external detector (APE GmbH, Berlin, Germany).
- Chameleon PreComp precompressor unit (Coherent, Milan, Italy).
- Optical power meter (PM100 with S121B sensor).
- LabVIEW (National Instruments, Austin, TX)-based application for CCD camera control and acquisition.
- LabVIEW (National Instruments, Austin, TX)-based application for spatial light modulator configuration.
- Calcium indicator Fluo-4AM (Invitrogen, Milan, Italy).
- MNI-glutamate (Tocris, Bristol, UK).

3. Methods

3.1. Combining an LCOS-SLM with a Commercial Two-Photon Laser Scanning Microscope

The LCOS-SLM has to be positioned in such way within the optical pathway of the microscope that the phase map generated by the LCOS-SLM is projected onto the back focal plane of the objective (Fig. 4). This optical design results in the projection, at the sample plane, of the Fourier transform distribution of the phase map generated by the LCOS-SLM. Given that, in commercial systems, the scan head galvo mirrors are usually optically conjugated to the back focal plane of the objective (via a 4f telescope composed of the tube lens/scan lens, Fig. 4) (38), LCOS-SLM conjugation with the pupil objective can be achieved by simply conjugating the LCOS-SLM with the galvo mirror plane (via a 4f telescope, Fig. 4). In 4f arrangement, the two lenses of the telescope are placed at distance equal to the sum of the two respective focal lengths. The image at the back focal plane of the first lens (L_3) is thereby relayed to the front focal plane of the second lens (L_4), with a magnification factor of f_4/f_3 (f_3 and f_4 respective focal lengths of L_3 and L_4). This optical design ensures the projection of the wave front generated by the LCOS-SLM onto the back focal plane of the objective without vignetting, thus avoiding the loss of high-frequency components located at the image periphery (39). Moreover, this strategy represents a

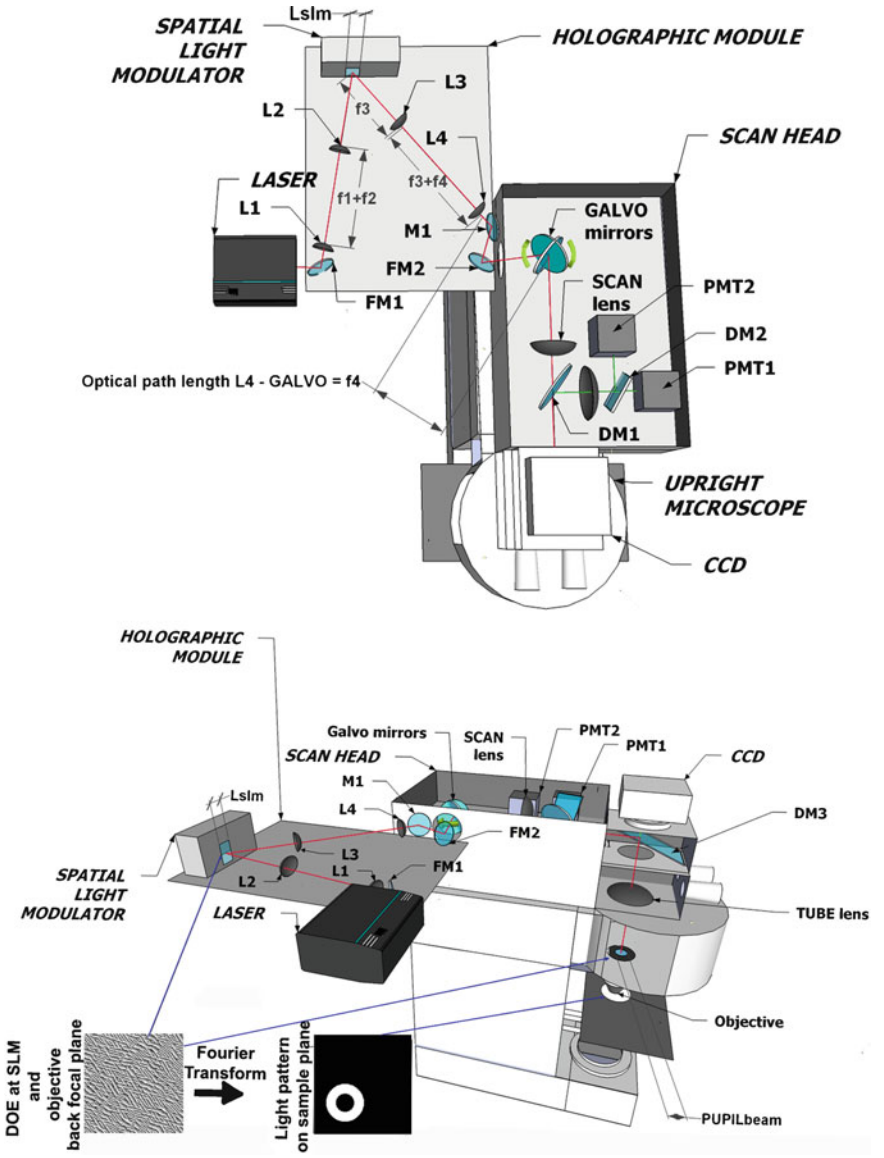

Fig. 4. Layout of the optical setup. *Legend*: FM_1, FM_2, flipping mirrors; M_1, turning mirror; L_1, L_2, L_3, L_4, plano-convex lenses; DM_1, 660-nm long-pass dichroic mirror; DM_2, 575-nm long-pass dichroic mirror; DM_3, 660-nm short-pass dichroic mirror; PMT_1, photomultiplier #1; PMT_2, photomultiplier #2; CCD, CCD camera.

convenient solution as scan heads are usually compact and difficult to modify with new optical components. The distance, d, between the LCOS-SLM and the galvo mirrors is thus:

$$d = 2f_3 + 2f_4.$$

The focal lengths of L_3 and L_4 are chosen to obtain the proper magnification of the beam diameter to match the dimension of the pupil of the microscope objective. Given the magnification of the

telescope composed of the scan and tube lens of the microscope (M_{MICR}), M_{T2} can be expressed as:

$$M_{T2} = \frac{f_4}{f_3} = \left(\frac{\emptyset_{PUPILbeam}}{\emptyset_{SLMbeam}}\right) \Big/ M_{MICR}$$

$$M_{MICR} = \frac{f_{tubelens}}{f_{scanlens}}$$

with $\emptyset_{PUPILbeam}$ being the diameter of the laser beam at the back aperture of the objective, $\emptyset_{SLMbeam}$ the diameter of the laser beam at the LCOS-SLM plane, and $f_{tubelens}$ and $f_{scanlens}$ the focal lengths of the tube and scan lenses, respectively, which are fixed characteristics of the scanning microscope. In some experimental configurations, a slight underfilling of the back aperture of the microscope objective may be preferred. This prevents the clipping out of the high-frequency content of the phase map and improves the light efficiency of the system, but results in a decrease in the effective numerical aperture of the objective (40). This might be useful for some photostimulation applications in which light efficiency is more important than spot size (31).

The diameter $\emptyset_{SLMbeam}$ of the beam impinging on the LCOS-SLM surface is determined by the lateral dimensions of the SLM surface (L_{SLM}, see also Fig. 4). It is recommended to maximize $\emptyset_{SLMbeam}$ in order to illuminate the maximum number of pixels of the LCOS-SLM chip, thereby increasing the high-frequency content of the projected diffractive optical element (DOE). With the help of a second telescope (lenses L_1 and L_2 in Fig. 4) between the laser and the LCOS-SLM, the diameter $\emptyset_{LASER}$ of the laser beam exiting the laser source is enlarged to $\emptyset_{SLMbeam}$. The magnification factor (M_{T1}) of this telescope is:

$$M_{T1} = \frac{f_2}{f_1} = \frac{\emptyset_{SLMbeam}}{\emptyset_{LASER}} = \frac{L_{SLM}}{\emptyset_{LASER}}.$$

The use of a cage assembly (Thorlabs Inc., Newton, NJ) to mount the telescopes is recommended as it simplifies their alignment. The correct alignment of the telescope is obtained by matching the laser spot position, in a plane far from the telescope, with and without the telescope lenses in the optical path.

3.2. Optimizing the Design of the Holographic Pathway

After defining the optical conjugation of the LCOS-SLM with the galvo mirrors of the scan head, a series of parameters must be considered to optimize the properties of the holographic path (see also Sects. 1 and 3). First, in order to achieve a compact and space-saving design, the LCOS-SLM position should be set close to the entrance port of the scan head. Second, the diffraction efficiency of the LCOS-SLM depends on the angle of incidence with which light impinges on it. To maximize the diffraction efficiency, the angle of incidence between the laser light and the

direction orthogonal to the LCOS-SLM plane should be kept to a minimum (as small as the dimensions of the optical components allow). Nonetheless, it should be considered that the angle of incidence also determines the distance at which the incident and reflected beam can be separated, thus determining the overall physical size of the holographic path. Smaller angles mean larger distances at which the two beams can be separated. An incidence angle of about 10° represents a good experimental compromise since it does not significantly affect the diffraction efficiency while allowing the separation of the two beams at a reasonable distance from the LCOS-SLM plane (e.g.: with a $Ø_{SLMbeam}$ of 10 mm, the two beams can be separated at about 10 cm from the LCOS-SLM). Third, it is recommendable to mount the LCOS-SLM onto two orthogonally positioned linear translators. In this way, the LCOS-SLM can be moved in a plane perpendicular to the direction of the laser propagation offering the possibility to center the position of the SLM chip on the laser beam without changing the angle of incidence.

3.3. Alignment of the Optical System

When redirecting the light going to the scan head onto the LCOS-SLM (mirror FM_1, Fig. 4), it is important to ensure that the laser beam is parallel to the optical table and centered in the optical axis of the light pathway. A convenient solution is to put the first (FM_1 in Fig. 4) and last (FM_2) mirrors of the holographic path on flip mounts to have the possibility to switch back and forth from the standard configuration of the scanning microscope to the holographic configuration. Moreover, the addition of a mirror (M_1) close to FM_2 facilitates the alignment of the beam in the scan head.

Once the holographic module is coupled to the scan head (see previous Sects. 1 and 2), it is necessary to fine-tune the alignment of the laser beam to the optical axis of the microscope. This aim can be achieved in eight steps as follows: (1) Ensure Köhler illumination with any kind of specimen, then remove the microscope objective and the sample, and set the galvo mirrors in their center position. (2) Close the field diaphragm of the halogen bulb to have a reference light spot at the objective housing port and center the laser beam on it (use mirrors M_1 and FM_2 to perform this task; FM_2 controls the laser position with respect to the reference spot while M_1 is used to center the light beam with respect to the entrance port of the scan head). (3) Repeat the same procedure with a microscope objective mounted on the microscope and a reflecting mirror at the sample plane while observing the shape of the reflected laser spot with a CCD camera mounted on the camera port. (4) Move FM_2 and M_1 sequentially to generate an undistorted laser spot at the center of field of view. Control the inclination of the laser beam with respect to the optical axis of the microscope with the same two mirrors (M_1 and FM_2) by

varying the focus of the objective (the laser spot changes in size but it should remain symmetric and in the same position in the images acquired with the CCD). (5) Switch on the SLM control unit and project a DOE to generate a grid of several spots evenly distributed on the sample plane. (6) Move the LCOS-SLM with the two orthogonal translators to center the projected DOE on the laser beam and obtain undistorted spots of similar intensity on the CCD. (7) In the center of the field of view, a bright spot, which represents the light component undiffracted by the LCOS-SLM (also called the "zero order"), is now visible. To remove the zero order component, different strategies can be used, including a reflecting grating to separate the first ($m = 1,-1$) from the zero order and the use of simple optical functions on the LCOS-SLM to direct only the diffracted portion of light to the scan head (41). Probably, one of the easiest methods to remove the zero order is by spatial filtering (25, 31). This can be done, for example, by placing a small piece of aluminum foil mounted on a glass coverslip at the Fourier plane of the first lens (L_3, Fig. 4) of the secondary telescope. This optical plane is conjugated to the sample plane and thus the projected hologram is visible, and the zero order can be filtered out by aligning the aluminum foil with the spot corresponding to the zero order component. (8) Adjust the distance of the lenses in one of the two telescopes to fine-tune the collimation of the beam. Put a fluorescent sample on the microscope stage (e.g., immunostained cells), flip down mirrors FM_1 and FM_2, and acquire a reference image with the scanning system and the PMTs. Flip mirrors FM_1 and FM_2 up and leave the LCOS-SLM switched off (the LCOS-SLM works as a reflecting mirror when turned off). Because in this configuration the laser is entering the scan head as a simple Gaussian beam, the scanning microscope works under normal conditions (raster scanning by galvo mirrors and images acquired with PMTs). During continuous imaging, fine-tune the distance between L_1 and L_2 to obtain the same focus position on the sample, as in the reference image (42).

3.4. Projecting Complex Spatial Light Patterns at the Sample Plane

At this point, it is possible to switch from a holographic scanless microscope to a laser scanning microscope by simply switching on/off the LCOS-SLM control unit without changing/removing any optical component. If the LCOS-SLM is switched on, it is possible to vary the field of view of the laser scanning system by changing the projected DOE on the LCOS-SLM. This procedure moves the position of the holographic spot at the sample plane, which is then raster scanned by the galvo mirrors. In this experimental configuration, phase-only modulation of the laser beam at the back focal plane of the microscope objective is obtained without altering the path of the beam within the scan head. In contrast, for scanless holographic imaging, it is necessary to direct emission light into the camera port. This is achieved by placing a

shortwave-pass dichroic mirror (DM_3, Fig. 4) to direct excitation light to the objective and the emission light to the CCD. Set a shortwave-pass emission filter to reject excitation light, and appropriate emission filters to select the emission bandwidth must then be placed in front of the CCD camera. It is now possible to project several holographic patterns at the sample plane (see Sect. 4 for details on the generation of the DOE) and acquire fluorescence signals at a frame rate limited only by the camera sensitivity.

3.5. Structured Light Illumination for Functional Imaging and Uncaging Experiments on Neuronal Networks

The light shaping properties achieved with holographic illumination allow the design of functional experiments that overcomes some of the major limitations of traditional wide-field and laser scanning approaches (see Sect. 1). Here, we first describe a protocol for holographic imaging of fluorescence signals on neuronal cultures at high acquisition rates and then a protocol for uncaging experiments with structured light illumination. We specifically focus on the procedures to optimize the optical setup while details on the preparation of neuronal cultures can be found elsewhere (43).

3.5.1. Imaging Experiment

In scanless imaging experiments, the LCOS-SLM can be used to tailor the laser light either into extended regions of interest or into a two-dimensional distribution of points according to the structure of the biological sample. When combined with the use of fluorescent reporter molecules, as for example the Ca^{2+} indicators Fluo-4 or Oregon Green BAPTA, this approach allows the simultaneous monitoring of specific neuronal subpopulations or subcellular compartments of a given cell at high acquisition frequencies. A high-resolution image of the biological sample is first obtained with the two-photon laser scanning system and PMTs; based on this, various regions of interest in the field of view are identified (Fig. 5a, see also Sect. 5). The experimental protocol then requires a brief calibration step, which depends on the selected working

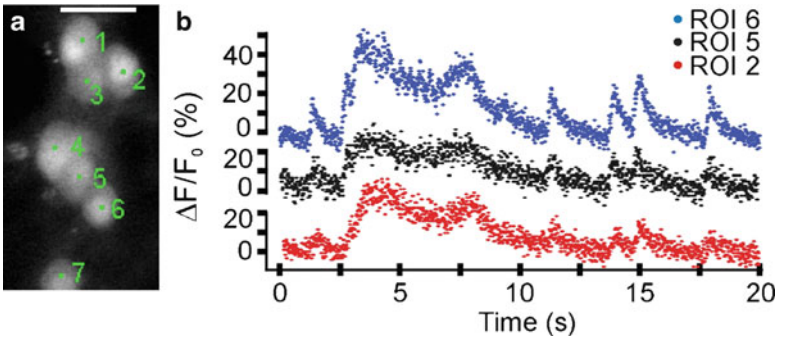

Fig. 5. Fast holographic Ca^{2+} imaging on neuronal networks. (**a**) Fluorescence image showing Fluo-4 loaded neurons in culture. Based on this image, multiple regions of interest corresponding to different cells (*green dots* numbered 1–7) are identified and simultaneously imaged with structured light ($\lambda_{imaging} = 830$ nm). *Scale bar* 15 μm. (**b**) Time course of the fluorescence signals showing spontaneous Ca^{2+} oscillations. Acquisition rate: 71 fps. Modified from (31).

wavelength, in order to establish a precise correspondence between the holographic addressable area and the PMT field of view. This can be achieved by projecting a phase mask corresponding, at the sample plane, to a reference gridded pattern while maintaining the galvo mirror in a reference position. Once the calibration procedure is performed, a simple software code can be used to extract the binary masks representing the desired illumination patterns from the images acquired in scanning mode. These patterns are then used to calculate the phase map to be sent to the LCOS-SLM control unit. Signals emitted from the different excited regions can then be collected in parallel by a fast CCD. Particular care has to be taken during high frame rate acquisition (>50 Hz) to find the best compromise between a good signal-to-noise ratio of the fluorescence signal variations and the power density that is continuously being delivered to the sample. Indeed, while the photodamage threshold limits the maximum power density per illuminated voxel at the sample plane, the signal of the emitted fluorescent light strongly depends upon the excitation power. As a reference, using two-photon excitation light at 830 nm, power density values of >10 mW per voxel have been reported to induce no photodamage during long-lasting Ca^{2+} recordings in brain slice preparation at frame rates around 60 fps (25). For similar acquisition rates, a power value of <4 mW per voxel has been used to measure Fluo-4 signals in neuronal cultures (Fig. 5b) (31).

3.5.2. Uncaging Experiment

The capability of shaping light into arbitrary three-dimensional illumination patterns with LCOS-SLM finds its natural application in photostimulation experiments, where light excitation is used to trigger conformational changes in synthetic molecules leading to the release of an effector molecule as, for example, in the case of MNI-glutamate uncaging. This approach can also be applied to light-gated proteins, as those of the opsin family, which can be expressed in neurons to control their excitability (35). The fine control of the three-dimensional and temporal profiles of the two-photon illumination that can be achieved with LCOS-SLM is fundamental to obtain reliable and effective stimulation while preserving the health of the preparation. Besides the specific working wavelengths, which depend upon the particular molecule that is photostimulated, the experimental protocol for photostimulation is similar to the one described for imaging experiments in terms of hardware configuration, calibration steps, and generation of phase maps. In photostimulation experiments though, a fine control of the illumination time interval and power density has to be performed. In the case of two-photon laser sources, this is achieved by introducing an electro-optic modulation unit, such as a Pockel cell, along the optical path (25, 31). The most important factor to be considered is the energy density required for photostimulation: at 720 nm (the optimal two-photon wavelength

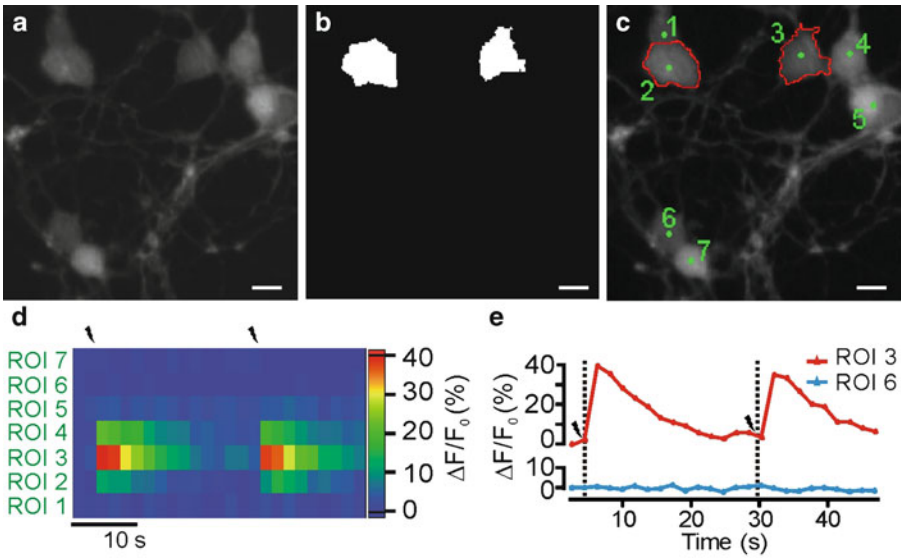

Fig. 6. Spatially defined activation of neurons with two-photon holographic uncaging of MNI-glutamate. (**a–c**) A fluorescence image of the field of view (**a**) is taken and used to generate an image mask (**b**) to configure the LCOS-SLM to illuminate only the desired regions of interest [*white regions* in (**b**) and areas delimited by a *red line* in (**c**)]. (**c**) Also shows the seven regions of interest in which Fluo-4 signals are monitored with conventional laser scanning microscopy at 0.54 Hz. (**d**, **e**) Time course of the Fluo-4 fluorescence. The *arrows* indicate the time of delivery of the photostimulus events. Modified from (31).

for MNI-glutamate uncaging), an energy density of about 10 μJ/μm^2 has been reported to be sufficient for the holographic illumination of cell body areas in neuronal cultures (Fig. 6) (31). At similar wavelengths, the recording of excitatory postsynaptic currents (EPSCs) in brain slices after spine stimulation required pulses with energy densities close to100 μJ/μm^2 (25). The electrophysiological recording of neuronal activity is undoubtedly the most sensitive and accurate method to track the photostimulus-induced effects with high temporal resolution (14, 25). Nonetheless, optical approaches for detecting the light-induced activity changes represent a valid alternative (24, 31).

4. Notes

4.1. Light Polarization

The LCOS-SLM is sensitive to the polarization of the incident light (see Sect. 3). It acts as a phase-only modulator for light that is linearly polarized in the direction corresponding to the liquid crystal orientation. Therefore, it is convenient to place a half-wave plate (RAC 5.2.10 achromatic $\lambda/2$ retarder—B. Halle Nachfl GmbH) between the laser source and the LCOS-SLM to linearly polarize the laser beam to match the LCOS-SLM optimal orientation, corresponding to the orientation of the liquid crystal director.

4.2. Generation of Three-Dimensional Patterns of Illumination

Another advantage of integrating a holographic apparatus into a scanning system is the ability to easily correct the z position of the excitation spot via software without the need of moving the objective while preserving the properties of the point spread function within a limited z range. This is obtained by imposing a phase map that produces a change in the collimation properties of the light beam (44). Thus, complex three-dimensional patterns of illumination can be generated.

4.3. Group Dispersion Velocity

An important aspect when using holographic illumination with multiphoton pulsed laser sources is the group velocity dispersion (GVD) introduced by the LCOS-SLM device. By using a CARPE autocorrelator (APEBerlin, Berlin, Germany), Dal Maschio et al. recently reported the broadening of femtosecond pulses generated by an LCOS-SLM-based holographic module (31). In the 760–980-nm range, the average GVD introduced by the holographic module with 20× objective (0.95 NA) is approximately 20,000 fs^2 at the sample plane, a value that can be completely compensated with commercial pulse compensators.

4.4. Configuration of the Diffractive Optical Element

A key aspect for the efficient use of LCOS-SLMs is the control and configuration of the liquid crystal active matrix. A phase map, also called DOE, has to be generated by a specific software. It is based on the desired illumination pattern at the sample plane and on the laser beam properties at the LCOS-SLM plane. Among the different algorithms available for holographic projection (45), the intuitive "Gratings and Lenses" approach and the versatile Gerchberg–Saxton algorithm are illustrated here. The Grating and Lenses model relies on the superposition of the phase characteristics of two basic optical components: gratings which produce lateral shifts and lenses which produce axial shifts. The capability of the gratings to steer a beam relies on the fact that the same wave-front modification induced by a linear phase profile, because of the 2π periodicity of a wave, can be obtained by decomposing it in a saw-tooth phase profile, where every period resembles the original 0–2π phase modulation (phase folding). Similarly, in the case of the axial shift, the change of the wave-front convergence position obtained by a lens is achieved by means of the projection of a circular phase map characterized by a periodic pattern with radial symmetry. The Grating and Lenses approach can also be used to generate multiple beams that can be independently controlled in a three-dimensional volume, but does not allow the projection of more complex and extended patterns at the sample plane (46). A more robust approach is the Gerchberg–Saxton algorithm (47), which is a Fourier transform-based method, that iteratively converges toward the phase distribution required at the LCOS-SLM plane to produce the desired intensity distribution at the sample plane. The algorithm is first initialized with a complex field with random phase and constant amplitude. By taking the

Fourier transform, a complex field at the image plane is then calculated. At this stage, the image field is modified preserving the phase information but substituting the calculated amplitude with the target amplitude distribution. In the following step, the resulting field is back propagated to the hologram plane by means of an Inverse Fourier Transform. The field resulting at the hologram plane is modified keeping the phase information but replacing the amplitude distribution with a constant distribution. After few iterations, the argument of the field at the hologram plane converges toward the phase map required to produce the target intensity at the sample plane. This algorithm can be used to generate multiple spots or even arbitrary two-dimensional distributions at the focal plane and can be integrated with the Grating and Lenses algorithm in order to achieve a multifocal projection of complex three-dimensional patterns.

4.5. Dimensions of the Holographic Field

At the sample plane, holographic illumination can be achieved generally in a subregion of the field of view (holographic field). The dimensions of the holographic field are determined by the maximum angle of deflection that is introduced by the LCOS-SLM. Theory sets this limit equal to:

$$u_{\max} = \frac{\lambda}{2 M_{T2} d_{\text{pitch}}} f_0,$$

where $u_{\max}$ is the maximum displacement of the laser spot on the sample plane, λ the wavelength of the laser source, d_{pitch} the pixel pitch of the LCOS-SLM chip, and f_o the focal length of objective (48). Diffraction efficiency of the device sets an experimental limit for $u_{\max}$.

4.6. Temporal Focusing

With the implementation of temporal focusing, the spectral components of a short laser pulse are geometrically dispersed by means of a grating to enhance the axial localization of the two-photon excitation (34, 41, 49). In this experimental configuration, a short pulse is obtained at the image plane of a lens projecting system while its shape is temporally stretched in the out-of-focus regions along the propagation direction (below and above the focal plane), leading to an effective two-photon absorption mostly limited to the focal plane. This optical design helps in preserving the z confinement of a bidimensional pattern with slow phase variations, but can lead to effective power reduction and to the broadening of the axial resolution improvement caused by DOE interference with the geometrical dispersion architecture (49).

Acknowledgments

We thank Gian Michele Ratto for critical reading of the manuscript. This work was supported by grants from MIUR PRIN program to F. Benfenati, Telethon-Italy (GGP09134 to F. Benfenati and GGP10138 to T. Fellin), and by the San Paolo "Programma in Neuroscienze" grant to F. Benfenati and T. Fellin.

References

1. Zhang J, Campbell RE, Ting AY et al (2002) Creating new fluorescent probes for cell biology. Nat Rev Mol Cell Biol 3:906–918
2. Giepmans BN, Adams SR, Ellisman MH et al (2006) The fluorescent toolbox for assessing protein location and function. Science 312:217–224
3. Kramer RH, Fortin DL, Trauner D (2009) New photochemical tools for controlling neuronal activity. Curr Opin Neurobiol 19:544–552
4. Gorostiza P, Isacoff E (2007) Optical switches and triggers for the manipulation of ion channels and pores. Mol Biosyst 3:686–704
5. Airan RD, Hu ES, Vijaykumar R et al (2007) Integration of light-controlled neuronal firing and fast circuit imaging. Curr Opin Neurobiol 17:587–592
6. Zhang F, Aravanis AM, Adamantidis A et al (2007) Circuit-breakers: optical technologies for probing neural signals and systems. Nat Rev Neurosci 8:577–581
7. Knopfel T, Lin MZ, Levskaya A et al (2010) Toward the second generation of optogenetic tools. J Neurosci 30:14998–15004
8. McManamon PF, Watson EA (2009) A review of phased array steering for narrow-band electrooptical systems. Proc IEEE 97:1078–1096
9. Savage N (2009) Digital spatial light modulators. Nat Photonics 3:170–172
10. Maurer C, Jesacher S, Bernet M et al (2011) What spatial light modulators can do for optical microscopy. Laser Photonics Rev 5:81–101
11. Tyson RK (1991) Principles of adaptive optics. Academic Press, London
12. Hardy JW (1998) Adaptive optics for astronomical telescopes. Oxford University Press, Oxford
13. Neil MA, Juskaitis R, Booth MJ et al (2000) Adaptive aberration correction in a two-photon microscope. J Microsc 200 (Pt 2):105–108
14. Lutz C, Otis TS, DeSars V et al (2008) Holographic photolysis of caged neurotransmitters. Nat Methods 5:821–827
15. Booth MJ (2007) Adaptive optics in microscopy. Philos Transact A Math Phys Eng Sci 365:2829–2843
16. Eriksen R, Daria V, Gluckstad J (2002) Fully dynamic multiple-beam optical tweezers. Opt Express 10:597–602
17. Melville H, Milne G, Spalding G et al (2003) Optical trapping of three-dimensional structures using dynamic holograms. Opt Express 11:3562–3567
18. van der Horst A, Forde NR (2008) Calibration of dynamic holographic optical tweezers for force measurements on biomaterials. Opt Express 16:20987–21003
19. Bowman R, Gibson G, Padgett M (2010) Particle tracking stereomicroscopy in optical tweezers: control of trap shape. Opt Express 18:11785–11790
20. Cojoc D, Difato F, Ferrari E et al (2007) Properties of the force exerted by filopodia and lamellipodia and the involvement of cytoskeletal components. PLoS One 2:e1072
21. Mejean CO, Schaefer AW, Millman EA et al (2009) Multiplexed force measurements on live cells with holographic optical tweezers. Opt Express 17:6209–6217
22. Ji N, Milkie DE, Betzig E (2010) Adaptive optics via pupil segmentation for high-resolution imaging in biological tissues. Nat Methods 7:141–147
23. Heintzman R (2010) Correcting distorted optics: back to the basic. Nat Photonics 7:108–110
24. Zahid M, Velez-Fort M, Papagiakoumou E et al (2010) Holographic photolysis for multiple cell stimulation in mouse hippocampal slices. PLoS One 5:e9431
25. Nikolenko V, Watson BO, Araya R et al (2008) SLM microscopy: scanless two-photon

imaging and photostimulation with spatial light modulators. Front Neural Circuits 2:5–19

26. Goldman JW (2005) Introduction to Fourier optics. Roberts & Company, Greenwood Village, CO
27. Khoo IA (2007) Liquid crystals. Wiley, Hoboken, NJ
28. Vicari L (2003) Optical applications of liquid crystals. Institute of Physics Publishing Ltd, London
29. Efron U (1994) Spatial light modulator technology: material, devices and applications. Marcel Dekker Inc., New York, NY
30. Dayton D, Browne S, Gonglewski J et al (2001) Characterization and control of a multielement dual-frequency liquid-crystal device for high-speed adaptive optical wave-front correction. Appl Opt 40:2345–2355
31. Dal Maschio M, Difato F, Beltramo R et al (2010) Simultaneous two-photon imaging and photo-stimulation with structured light illumination. Opt Express 18:18720–18731
32. Nikolenko V, Peterka DS, Yuste R (2010) A portable laser photostimulation and imaging microscope. J Neural Eng 7:045001
33. Peron S, Svoboda K (2011) From cudgel to scalpel: toward precise neural control with optogenetics. Nat Methods 8:30–34
34. Andrasfalvy BK, Zemelman BV, Tang J et al (2010) Two-photon single-cell optogenetic control of neuronal activity by sculpted light. Proc Natl Acad Sci USA 107:11981–11986
35. Papagiakoumou E, Anselmi F, Begue A et al (2010) Scanless two-photon excitation of channelrhodopsin-2. Nat Methods 7:848–854
36. Palima D, Alonzo CA, Rodrigo PJ et al (2007) Generalized phase contrast matched to Gaussian illumination. Opt Express 15:11971–11977
37. Gluckstad J, Palima D (2010) Generalized phase contrast. Springer in association with Canopus Academic Publishing Limited, Dordrecht, NE
38. Lee WM, Reece PJ, Marchington RF et al (2007) Construction and calibration of an optical trap on a fluorescence optical microscope. Nat Protoc 2:3226–3238
39. Martin-Badosa E, Montes-Usategui M, Carnicer A et al (2007) Design strategies for optimizing holographic optical tweezers setups. J Opt A Pure Appl Opt 9:S267–S277
40. Helmchen F, Denk W (2005) Deep tissue two-photon microscopy. Nat Methods 2:932–940
41. Papagiakoumou E, de Sars V, Oron D et al (2008) Patterned two-photon illumination by spatiotemporal shaping of ultrashort pulses. Opt Express 16:22039–22047
42. Shaevitz JW, Fletcher DA (2007) Enhanced three-dimensional deconvolution microscopy using a measured depth-varying point-spread function. J Opt Soc Am A Opt Image Sci Vis 24:2622–2627
43. Doering LC (2010) Protocols for neural cell culture. Springer, Heidelberg
44. Daria VR, Stricker C, Bowman R et al (2009) Arbitrary multisite two-photon excitation in four dimensions. Appl Phys Lett 95:093701-1–093701-3
45. Liesener J, Reicherter M, Haist T et al (2000) Multi-functional optical tweezers using computer-generated holograms. Opt Commun 185:77–82
46. Leach J, Wulff K, Sinclair G et al (2006) Interactive approach to optical tweezers control. Appl Opt 45:897–903
47. Zalevsky Z, Mendlovic D, Dorsch RG (1996) Gerchberg–Saxton algorithm applied in the fractional Fourier or the Fresnel domain. Opt Lett 21:842–844
48. Golan L, Reutsky I, Farah N et al (2009) Design and characteristics of holographic neural photo-stimulation systems. J Neural Eng 6:066004
49. Papagiakoumou E, de Sars V, Emiliani V et al (2009) Temporal focusing with spatially modulated excitation. Opt Express 17:5391–5401